Journal of Materials Chemistry A

ROYAL SOCIETY OF CHEMISTRY

PAPER

View Article Online
View Journal | View Issue

Cite this: J. Mater. Chem. A, 2020, 8, 9726

The rational and effective design of nonfullerene acceptors guided by a semi-empirical model for an organic solar cell with an efficiency over 15%†

Xin Ke,‡ Lingxian Meng,‡ Xiangjian Wan, * Mingpeng Li, Yanna Sun, Ziqi Guo, Simin Wu, Hongtao Zhang, Chenxi Li and Yongsheng Chen

Received 18th March 2020
Accepted 24th April 2020

DOI: 10.1039/d0ta03087b

rsc.li/materials-a

Although much progress has been made in the field of organic photovoltaics (OPVs), the design of active layer materials is generally based on a trial-and-error approach. It is still a challenge to rationally design active layer materials to further improve OPV performance. Herein, guided by a semi-empirical model that we have proposed, two new small-molecule acceptors, named F-2F and FO-2F, were designed and synthesized based on the acceptor F-H. F-2F, having a difluoro-substituted end group, showed absorption red-shifted relative to that of F-H, but still far from the range required in the semi-empirical model. Thus, we performed subtle molecular optimization by inserting an oxygen atom into the backbone of F-2F to design FO-2F, which exhibited much greater red-shifted absorption, close to the preferred absorption range of the semi-empirical model. When blended with the donor polymer PM6, an OPV device based on FO-2F achieved an impressive PCE of 15.05% with a V_{oc} of 0.878 V, a J_{sc} of 22.26 mA cm^{-2} and a notable FF of 0.77. Both the V_{oc} and J_{sc} values were within the predicted range of the model. These results showed the FO-2F molecule to be a new example of an acceptor yielding a PCE greater than 15%, an achievement previously restricted nearly entirely to the Y6 series.

Introduction

Organic photovoltaics (OPVs) have attracted great attention as forming one of the most promising classes of renewable energy platforms owing to their advantages of low cost, light weight, flexibility and roll-to-roll manufacturing capability.[1–3] In the past few years, ever better power conversion efficiencies (PCEs) of OPVs have been frequently reported, and have reached exciting values of 16–18%.[4–16] These remarkable results are mainly attributed to the design of new and better active layer materials, together with improved understanding of the OPV mechanism and device optimization.[17–21] Notably, with their easily tunable absorption and energy levels, nonfullerene acceptors (NFAs), especially small molecules with the acceptor–donor–acceptor (A–D–A) architecture, have played a critical role to boost the performance of OPVs.[22–31] In fact, the star NFA Y6 could also be arguably regarded as an A–D–A-type molecule, based on careful comparisons of its electron cloud distribution with those of other typical A–D–A molecules such as ITIC, 5T, and F-H.[4,32–35] To date, except for only a very few cases,[36–38] the OPV devices with efficiency values of over 15% are all based on Y6 and its derivatives.[4–7,10,11,13,39–41] Although PCEs of 16–18% have been achieved for Y6-based devices, there is still much room for improving OPV performance according to many theoretical predictions.[14,42,43] In addition, in the view of the vast diversity of chemical structures of organic materials, there is no doubt that more molecules yielding performances better than those of Y6 derivatives could be designed through rational design.[14,35,38,44,45]

Previously, we presented a semi-empirical model to predict the PCEs of two terminal tandem OPVs and have used it as an effective guideline for the screening of active layer materials and design of tandem devices.[14] In fact, the semi-empirical model can also be used to design active layer materials for single-junction devices (see details in ESI†). As shown in Fig. 1a, a high efficiency of 20% could be reached for a single-junction device if all of the parameters, including fill factor (FF), open-circuit voltage (V_{oc}), short-circuit current density (J_{sc}), and voltage loss (E_{loss}), could be optimized simultaneously. For example, with an E_{loss} of 0.55 eV, an average value for state-of-the-art OPVs,[6,7,38] PCEs of 16–18% can be achieved with an active layer absorption onset (λ_{onset}) of about 860–930 nm, average EQE of 70–80% and FF of 80%. Note the desired optimal parameters include a V_{oc} of 0.89–0.78 V and J_{sc} of 22.13–28.20 mA cm^{-2}. Clearly, absorption onset should be the first parameter considered when designing the molecule, in particular

State Key Laboratory and Institute of Elemento-Organic Chemistry, The Centre of Nanoscale Science and Technology, Key Laboratory of Functional Polymer Materials, Renewable Energy Conversion and Storage Center (RECAST), College of Chemistry, Nankai University, Tianjin, 300071, China. E-mail: xjwan@nankai.edu.cn

† Electronic supplementary information (ESI) available. See DOI: 10.1039/d0ta03087b

‡ X. K. and L. M. contributed equally.

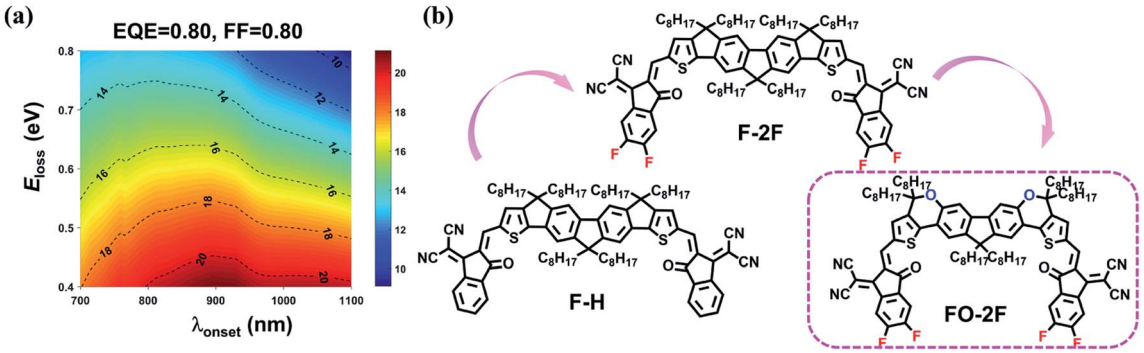

Fig. 1 (a) Predicted PCEs *vs.* E_{loss} and active layer absorption onset (λ_{onset}), with an assumed average EQE of 80% and FF of 0.80 for single-junction OPVs based on semi-empirical analysis (see ref. 14 and ESI† for more details). (b) The chemical structures of F-2H, F-2F and FO-2F.

since other parameters such as E_{loss}, EQE and FF are directly related to device fabrication and optimization. Furthermore, as shown in Fig. 1a, there exists a trade-off between E_{loss} and absorption onset, which can affect V_{oc} and J_{sc}. Although the detailed mechanism behind E_{loss} remains unclear, much progress has been made in this regard and has shown that the energy offset between donor and acceptor materials plays a critical role for E_{loss}.[46] Therefore, controlling the energy levels of the donor and acceptor in the active layers should be considered simultaneously. Of course, controlling the morphology is as important as controlling the absorption and energy levels, but is still a great challenge for the OPV community.[47,48] While the device results of the Y6 series are quite consistent with the above model analysis, it is worth noting that there is still much room for achieving better material design according to comparisons of the parameters of Y6 with the optimal ones obtained based on the semi-empirical analysis.

In one of our previous works, we designed an acceptor, named FDICTF (F-H),[35] displaying a PCE of 10.06%, a V_{oc} of 0.94 V, a J_{sc} of 15.81 mA cm^{-2} and an FF of 0.66. The λ_{onset} of F-H was shown to be ~760 nm, which is the main limit for its performance according to the above semi-empirical analysis. In fact, using the semi-empirical model, its derivative F-M was designed and successfully used as the front cell material in the fabrication of a high-performance tandem solar cell with a PCE of 17.3%.[14] From the perspective of single-junction devices, F-H displays a high V_{oc} and FF, but its λ_{onset} of 760 nm is far from the preferred absorption range of 860–930 nm. For the state-of-the-art NFA-based OPVs, the donor and acceptor absorb light at the short- and long-wavelength regions, respectively. Thus, the absorption onset of the active layer is determined by the acceptor—and F-H hence has the potential to be used as a "leading compound" to design better acceptors for high-efficiency single-junction devices if its absorption can be red-shifted to the preferred range, while keeping a balanced V_{oc} and maintaining or improving the FF.

Bearing these issues in mind, we designed two A–D–A-type molecules, denoted as F-2F and FO-2F, from F-H based on the guidelines of the above semi-empirical model (Fig. 1b). By introducing a difluoro-substituted end group to obtain F-2F[26,28,49] and further inserting an oxygen atom into the backbone of F-2F to obtain FO-2F,[50–55] the λ_{onset} was shifted from 760 to 776 and 845 nm successively, with this 845 nm value being very close to the preferred values for high-performance single-junction devices. Note one principle in our design was that we aimed to make minimum changes to the structure, particularly to the molecular backbone, as the initial compound F-H had already demonstrated a promising device performance with a high V_{oc} and decent FF, albeit relatively low J_{sc} owing to the inefficient absorption range with an λ_{onset} of 760 nm.[35] Following this principle would make it more likely that the new molecules have morphologies similar to that of F-H and thus maintain the high fill factor and low E_{loss}. Indeed, as expected, with device optimization, the FO-2F-based OPV achieved an impressive PCE of 15.05% with a V_{oc} of 0.878 V, a J_{sc} of 22.26 mA cm^{-2} and a notable FF of 0.77, when combined with the suitable donor material PM6. These results demonstrated that high-performance active layer materials can be designed based on the guidelines of the semi-empirical model.

Results and discussion

Syntheses and thermal properties

The synthetic routes to F-2F and FO-2F are shown in Scheme S1.† The detailed procedures and characterizations are summarized in ESI.† The chemical structures of F-2F and FO-2F were characterized and confirmed from the results of ^{1}H/^{13}C nuclear magnetic resonance (NMR) spectroscopy and high-resolution mass spectrometry (HRMS) analyses. These two molecules exhibited good levels of solubility in common organic solvents, such as dichloromethane, chloroform and chlorobenzene. According to acquired thermogravimetric analysis (TGA) curves, shown in Fig. S2,† F-2F and FO-2F showed good thermal stability with high decomposition temperatures (T_d) of 327 and 329 °C, respectively.

Optical absorption and electrochemical properties

The ultraviolet-visible (UV-vis) absorptions of F-H, F-2F and FO-2F in chloroform solution and thin film are shown in Fig. 2a and S3,† and some detailed data are summarized in Table 1. As shown in Fig. S3,† F-2F in a chloroform solution exhibited an

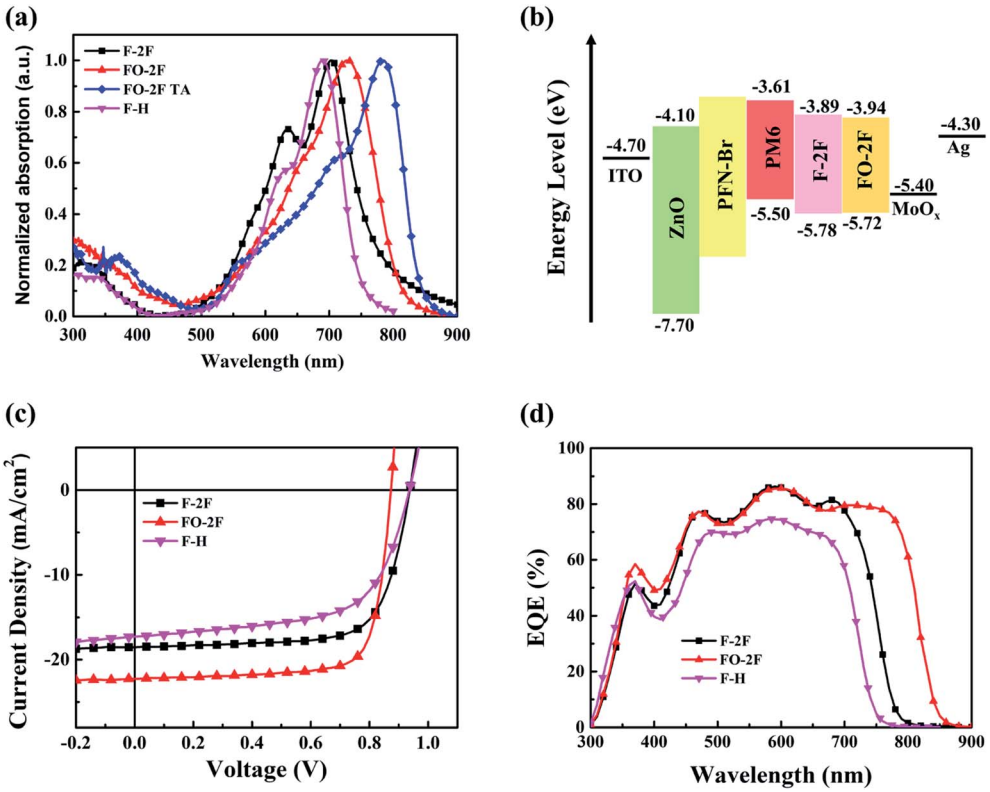

Fig. 2 (a) Normalized absorption spectra of the as-cast films of F-H and F-2F, and the TA film of FO-2F. (b) Energy level diagram of the solar cell. (c) Current density–voltage (J–V) and (d) EQE curves of the optimized devices.

absorption peak (λ_{max}) at 678 nm, clearly red-shifted compared with that of F-H (λ_{max} = 665 nm). The solution of FO-2F, having further an O inserted in the bridge unit, showed a more red-shifted absorption, with a λ_{max} of 696 nm. Compared with their solution absorptions, the absorptions of the as-cast solid films of F-2F and FO-2F were substantially red-shifted, by 25 and 32 nm, with their absorption onsets (λ_{onset}) shifted to 776 and 813 nm, respectively. Though the λ_{onset} values of these two materials were still not close to the preferred values indicated in the semi-empirical model, the FO-2F film showed a further red-shifted absorption, by 56 nm, after thermal annealing (TA), with its λ_{onset} shifted to 845 nm. Note that this λ_{onset} was quite close to the preferred values required for high-performance single-junction cells as indicated in the model analysis above (Fig. 1a). The significant redshift after annealing was ascribed to the strong and ordered molecular packing of FO-2F as discussed below. Interestingly, the F-2F film unexpectedly showed no clear redshift after TA treatment. The absorption spectra of PM6:F-2F and PM6:FO-2F blend films are shown in Fig. S4.†

The energy levels of F-2F and FO-2F were investigated by taking electrochemical cyclic voltammetry measurements (Fig. S5†). As shown in Table 1, the HOMO/LUMO levels for F-2F and FO-2F were determined to be −5.78/−3.89 and −5.72/−3.94 eV, respectively. Compared with those of F-H (−5.43/−3.71 eV), the energy levels of F-2F and FO-2F were found to be all downshifted, with and the bandgap having become narrower as expected.[26,28,49] These results were consistent with the calculated HOMO/LUMO energy levels of F-2F (−5.65/−3.45 eV) and FO-2F (−5.55/−3.48 eV), respectively.

Meanwhile, theoretical calculations were performed using density functional theory (DFT) at the B3LYP/6-31G* level to study their optimal geometric configurations. The results of these calculations showed both F-2F and FO-2F adopting conformations, including planar backbones, quite similar to

Table 1 Optical and electrochemical data for F-H, F-2F and FO-2F

Comp.	λ_{max}^{sol} [nm]	λ_{max}^{film} [nm]	HOMO [eV]	LUMO [eV]	λ_{onset} [nm]	E_g^{opta} [eV]
F-H[b]	665	689	−5.43[b]	−3.71[b]	760	1.63
F-2F	678	703	−5.78	−3.89	776	1.60
FO-2F	696	728 (784)[c]	−5.72	−3.94	845	1.47

[a] The optical bandgap estimated from the absorption onset. [b] Data were obtained from ref. 35. [c] Absorption data with TA at 130 °C for 10 min.

those of F-H (Fig. S6†), following our design principle mentioned above of minimizing structural changes and maintaining similar morphologies for these molecules in the solid state.

Photovoltaic properties

To evaluate the photovoltaic properties of F-2F and FO-2F, OPV devices using them as active layers were fabricated with an inverted structure of indium tin oxide (ITO)/ZnO/PFN-Br/active layer/MoO_x/Ag (Fig. 2b). PM6 was selected as the donor due to its absorption being complementary to, and its energy levels matching, those of the two acceptors. The detailed results for device optimization are provided in ESI (Tables S1 and S2);† the optimal weight ratio of donor to acceptor was 1 : 1. The optimized photovoltaic parameters of F-2F and FO-2F together with that for F-H as comparison are summarized in Table 2, and the corresponding *J–V* characteristics are shown in Fig. 2c. As shown in Table 2, the optimized F-2F-based device showed a PCE of 12.93% with a V_{oc} of 0.941 V and J_{sc} of 18.54 mA cm^{-2}. A significantly higher PCE of 15.05%, with a V_{oc} of 0.878 V, high J_{sc} of 22.26 mA cm^{-2} and notable FF of 77.0%, was achieved for the FO-2F-based device. These results showed the performances of F-2F and especially FO-2F, along with those of the Y6 series, to be among the best in this field.

The considerably better performance displayed by FO-2F than by F-H and F-2F deserves some discussion. As described above, the main limit for F-H has been indicated to be its absorption. By introducing F into the end group and inserting O into the backbone, the absorption was red-shifted significantly, with λ_{onset} changing from 760 to 776 and 845 nm successively, and correspondingly J_{sc} becoming much enhanced (from 15.81 for F-H to 18.54 for F-2F and 22.26 mA cm^{-2} for FO-2F). The V_{oc} values measured for these three compounds were 0.940, 0.941 and 0.878 V, respectively. The relatively poor V_{oc} for FO-2F, compared to that for F-H, was made up for by its relatively good J_{sc}. It is worth noting that the FFs resulting from these three compounds were found to be similar, albeit with modestly higher values for F-2F and especially FO-2F, attributed to the similarities in their structures and morphologies (discussed below). Taken together, the final designed compound FO-2F demonstrated values of the parameters λ_{onset}, FF, V_{oc}, J_{sc} overall close to those of the desired optimal materials discussed above.

The improved and high performances of F-2F and especially FO-2F, relative to that of F-H, were also indicated by their external quantum efficiency (EQE) levels, shown in Fig. 2d. The high J_{sc} of the FO-2F-based device was attributed to its efficient photo-electron response up to the region of ~850 nm, comparing to only 760 nm for F-H and 776 nm for F-2F. Thus, relative to that of the F-H device, the integrated J_{sc} values of the F-2F and FO-2F devices determined from the EQE curves were improved to 18.06 and 21.61 mA cm^{-2}, respectively, values in good agreement with the J_{sc} values from the *J–V* measurements, and the deviations were within 5%.

The charge generation and charge recombination behavior in the optimal PM6:F-2F- and PM6:FO-2F-based devices were also investigated. Curves of photocurrent (J_{ph}) *versus* effective applied voltage (V_{eff}) were acquired, and are shown in Fig. 3a. The charge dissociation probability could be estimated with the value of J_{ph}/J_{sat}.[56] Under short-circuit conditions, the J_{ph}/J_{sat} values for the F-2F- and FO-2F-based devices were determined to be 97% and 96%, respectively. Under maximal power output conditions, the values of J_{ph}/J_{sat} were both 87% for the F-2F- and FO-2F-based devices. These values are higher than those for the F-H-based device[57] (91% under short-circuit conditions and 74% under maximal power output conditions). The results demonstrated more effective exciton dissociation and charge collection for the F-2F- and FO-2F-based devices. In order to further study the charge recombination properties in the devices, the light-intensity (*P*) dependence of J_{sc} was also measured[56] (Fig. 3b). The α values for the devices based on F-2F and FO-2F were determined to be 0.984 and 0.991, respectively, higher than that of the F-H-based devices (0.957).[57] According to the power-law equation $J_{sc} \propto P^{\alpha}$, the α values close to 1 indicated that bimolecular recombination was effectively suppressed in the F-2F- and FO-2F-based devices, supporting the high FF values of these materials. In order to gain an increased understanding of the recombination processes, the dependence of V_{oc} on light intensity was also examined. A slope close to kT/q (where k is the Boltzmann constant, T is the temperature in Kelvin, and q is the elementary charge) is generally indicative of a negligible amount of trap-assisted recombination. As shown in Fig. S7,† the PM6:F-2F- and PM6:FO-2F-based devices showed slopes of 1.42 kT/q and 1.37 kT/q, respectively. These results thus indicated lower amounts of trap-assisted recombination losses for the PM6:FO-2F-based device.

The charge mobilities of the PM6:F-2F and PM6:FO-2F blend films were measured by following the space-charge-limited current (SCLC) method (Fig. S8†). The PM6:F-2F and PM6:FO-2F photoactive layers exhibited hole/electron mobility values of $2.86 \times 10^{-4}/1.48 \times 10^{-4}$ and $5.30 \times 10^{-4}/2.43 \times 10^{-4}$ cm^2 V^{-1} s^{-1}, respectively, values higher than those of the F-H-based device ($3.37 \times 10^{-5}/2.40 \times 10^{-5}$ cm^2 V^{-1} s^{-1}).[57] The higher hole and electron mobilities of PM6:FO-2F were consistent with the increased FF of the PM6:FO-2F-based devices.

Table 2 Photovoltaic parameters of F-2F-, FO-2F- and F-H-based optimized devices under AM 1.5G (100 mW cm^{-2}) illumination

Device	V_{oc} [V]	J_{sc} [mA cm^{-2}]	FF%	PCE%	E_{loss} (eV)
F-2F	0.941	18.54	74.1	12.93 (12.75)[a]	0.66
FO-2F	0.878	22.26	77.0	15.05 (14.69)[a]	0.59
F-H[b]	0.940	15.81	66.0	10.06 (9.81)	0.69

[a] The average PCEs provided in parentheses were obtained from 10 devices. [b] Data were obtained from ref. 35.

Morphology characterization

The morphologies of the PM6:F-2F and PM6:FO-2F blend films were studied by carrying out tapping-mode atomic force microscopy (AFM) and transmission electron microscopy (TEM) analyses. In the AFM images (Fig. 4), the PM6:F-2F and PM6:FO-

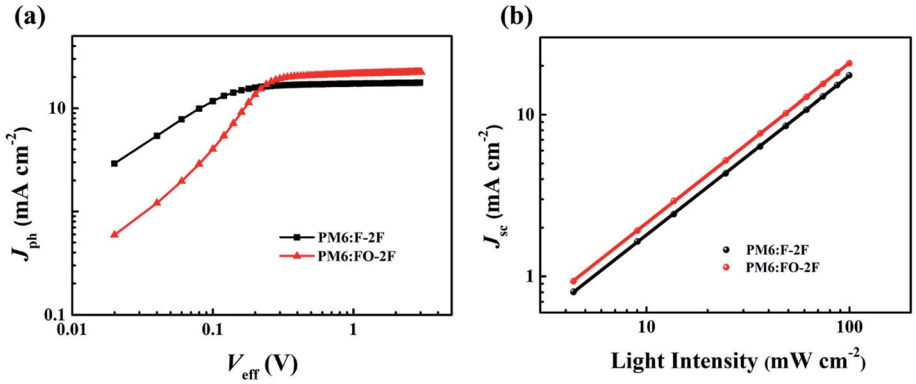

Fig. 3 (a) J_{ph} *versus* V_{eff} and (b) J_{sc} *versus* light intensity (*P*) for the optimized F-2F- and FO-2F-based devices.

2F films were observed to display a finely dispersed phase separation with low root-mean-square surface roughness values of 2.21 and 1.94 nm, lower than that of the F-H-based film (3.40 nm).[57] Furthermore, in the TEM images, both of these blend films displayed obvious fiber-like interpenetrating network nanostructures, similar to those displayed by the F-H based film, with such nanostructures benefiting exciton dissociation and charge transport. A line cut of a grazing-incidence wide-angle X-ray scattering (GIWAXS) pattern of a FO-2F film not subjected to TA showed a weak differentiation peak (Fig. S9†). This peak became stronger after TA, implying a more ordered packing of the molecules in the FO-2F film after TA. F-2F and FO-2F neat films after TA showed π–π stacking diffraction peaks (010) at 1.81 and 1.90 Å^{-1}, corresponding to π–π

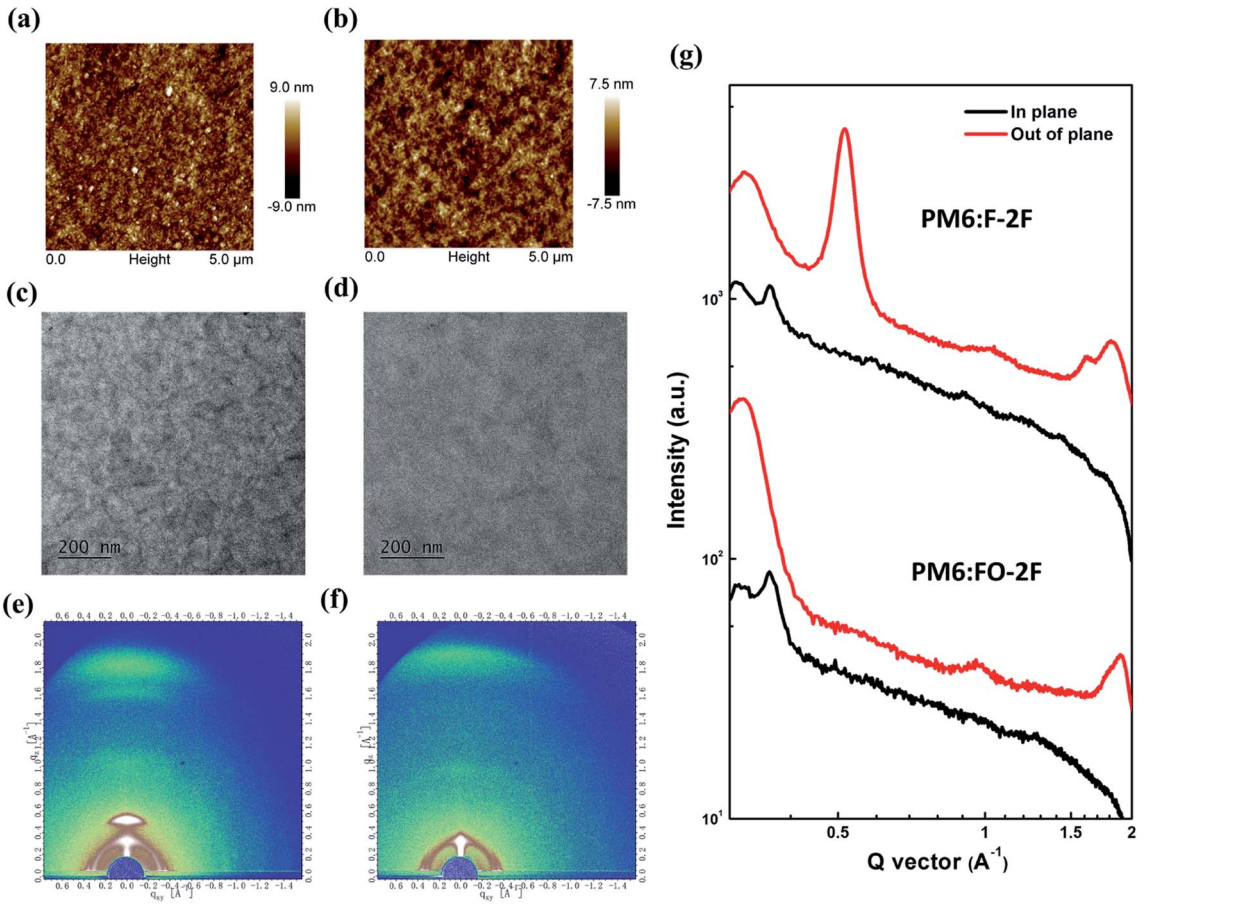

Fig. 4 (a and b) AFM and (c and d) TEM images of (a and c) the PM6:F-2F blend film and (b and d) PM6:FO-2F blend film. Each scale bar corresponds to 200 nm. (e and f) GIWAXS patterns of (e) the PM6:F-2F blend and (f) PM6:FO-2F blend. (g) In-plane and out-of-plane line cuts of the corresponding GIWAXS patterns.

distances of 3.47 and 3.30 Å, respectively. This result indicated an enhanced molecular packing for F-2F and FO-2F in their solid films compared with that of F-H, for which a π–π distance of 3.53 Å has been reported.[57] For the PM6:F-2F and PM6:FO-2F blend films (Fig. 4e and f), clear face-on diffraction peaks were observed at, respectively, 1.82 and 1.89 $Å^{-1}$ in the out-of-plane (OOP) direction, corresponding to similar π–π stacking distances of 3.46 and 3.32 Å, respectively. As shown in Table S3,† the crystal coherence lengths (CCLs) in the (010) region for the F-2F- and FO-2F-based blend films were calculated from the Scherrer equation (CCL = $2\pi k$/fwhm)[58] to be 31.5 and 49.5 Å, respectively, greater than that of the F-H-based film (16.2 Å).[59] The strong π–π stacking of F-2F and FO-2F along with the increased CCL were beneficial for charge transport, consistent with the high electron mobilities and improved photovoltaic performances of these two new designed acceptors compared with that of F-H. Clearly, modification of the starting compound F-H to produce the new F-2F and FO-2F acceptors maintained or even improved the originally high-quality packing and morphology. These results indicated that minimum changes to the chemical structure should be considered for designing higher-performance molecules from already well-performing molecules under the guide of our semi-empirical model.

Conclusions

In summary, we have designed and synthesized two new small-molecule acceptors, F-2F and FO-2F, under the guidelines of a semi-empirical model. Both F-2F and FO-2F showed absorption red-shifted compared with that of the initial F-H molecule, with the absorption onset (λ_{onset}) red-shifted to 776 and 845 nm, respectively. This λ_{onset} of FO-2F was very similar to the optimal values suggested by the semi-empirical model, with this similarity endowing this molecule with a much improved and high J_{sc} of 22.26 mA cm^{-2} when combined with the donor PM6. Together with the corresponding optimal V_{oc} of 0.878 V and FF of 0.77, the FO-2F-based devices demonstrated a PCE of 15.05%, a performance level only second to those of the Y6 series molecules. These results indicated that higher-performance molecules could be designed and achieved starting from already well-performing molecules by using our semi-empirical model as a guide, provided that the structures of the chosen starting molecules are largely maintained.

Conflicts of interest

There are no conflicts to declare.

Acknowledgements

The authors gratefully acknowledge financial support obtained from MoST (2019YFA0705900, 2016YFA0200200), NSFC (21935007, 51773095 and 51873089) of China, Tianjin City (17JCJQJC44500) and the 111 Project (B12015). The authors also thank the staff at beam line 1W1A of the Beijing Synchrotron Radiation Laboratory Institute of High Energy Physics for providing the beam time.

References

1 Z. Li, G. He, X. Wan, Y. Liu, J. Zhou, G. Long, Y. Zuo, M. Zhang and Y. Chen, *Adv. Energy Mater.*, 2012, **2**, 74–77.
2 G. Yu, J. Gao, J. C. Hummelen, F. Wudl and A. J. Heeger, *Science*, 1995, **270**, 1789–1791.
3 F. C. Krebs, *Sol. Energy Mater. Sol. Cells*, 2009, **93**, 394–412.
4 J. Yuan, Y. Zhang, L. Zhou, G. Zhang, H.-L. Yip, T.-K. Lau, X. Lu, C. Zhu, H. Peng, P. A. Johnson, M. Leclerc, Y. Cao, J. Ulanski, Y. Li and Y. Zou, *Joule*, 2019, **3**, 1140–1151.
5 B. Fan, D. Zhang, M. Li, W. Zhong, Z. Zeng, L. Ying, F. Huang and Y. Cao, *Sci. China: Chem.*, 2019, **62**, 746–752.
6 Y. Cui, H. Yao, J. Zhang, T. Zhang, Y. Wang, L. Hong, K. Xian, B. Xu, S. Zhang, J. Peng, Z. Wei, F. Gao and J. Hou, *Nat. Commun.*, 2019, **10**, 2515.
7 X. Xu, K. Feng, Z. Bi, W. Ma, G. Zhang and Q. Peng, *Adv. Mater.*, 2019, **31**, 1901872.
8 K. Li, Y. Wu, Y. Tang, M. A. Pan, W. Ma, H. Fu, C. Zhan and J. Yao, *Adv. Energy Mater.*, 2019, **9**, 1901728.
9 Q. An, X. Ma, J. Gao and F. Zhang, *Sci. Bull.*, 2019, **64**, 504–506.
10 K. Jiang, Q. Wei, J. Y. L. Lai, Z. Peng, H. K. Kim, J. Yuan, L. Ye, H. Ade, Y. Zou and H. Yan, *Joule*, 2019, **3**, 3020–3033.
11 J. Xiong, K. Jin, Y. Jiang, J. Qin, T. Wang, J. Liu, Q. Liu, H. Peng, X. Li, A. Sun, X. Meng, L. Zhang, L. Liu, W. Li, Z. Fang, X. Jia, Z. Xiao, Y. Feng, X. Zhang, K. Sun, S. Yang, S. Shi and L. Ding, *Sci. Bull.*, 2019, **64**, 1573–1576.
12 L. Hong, H. Yao, Z. Wu, Y. Cui, T. Zhang, Y. Xu, R. Yu, Q. Liao, B. Gao, K. Xian, H. Y. Woo, Z. Ge and J. Hou, *Adv. Mater.*, 2019, **31**, 1903441.
13 Q. Liu, Y. Jiang, K. Jin, J. Qin, J. Xu, W. Li, J. Xiong, J. Liu, Z. Xiao, K. Sun, S. Yang, X. Zhang and L. Ding, *Sci. Bull.*, 2020, **65**, 272–275.
14 L. Meng, Y. Zhang, X. Wan, C. Li, X. Zhang, Y. Wang, X. Ke, Z. Xiao, L. Ding, R. Xia, H.-L. Yip, Y. Cao and Y. Chen, *Science*, 2018, **361**, 1094–1098.
15 F. Huang, *Acta Polym. Sin.*, 2018, 1141–1143.
16 X. Ma, J. Wang, Q. An, J. Gao, Z. Hu, C. Xu, X. Zhang, Z. Liu and F. Zhang, *Nano Energy*, 2020, **70**, 104496.
17 G. Zhang, J. Zhao, P. C. Y. Chow, K. Jiang, J. Zhang, Z. Zhu, J. Zhang, F. Huang and H. Yan, *Chem. Rev.*, 2018, **118**, 3447–3507.
18 O. Ostroverkhova, *Chem. Rev.*, 2016, **116**, 13279–13412.
19 K. Gao, S. B. Jo, X. Shi, L. Nian, M. Zhang, Y. Kan, F. Lin, B. Kan, B. Xu, Q. Rong, L. Shui, F. Liu, X. Peng, G. Zhou, Y. Cao and A. K. Jen, *Adv. Mater.*, 2019, **31**, 1807842.
20 J. Gao, W. Gao, X. Ma, Z. Hu, C. Xu, X. Wang, Q. An, C. Yang, X. Zhang and F. Zhang, *Energy Environ. Sci.*, 2020, **13**, 958–967.
21 X. Ma, Q. An, O. A. Ibraikulov, P. Lévêque, T. Heiser, N. Leclerc, X. Zhang and F. Zhang, *J. Mater. Chem. A*, 2020, **8**, 1265–1272.
22 Y. Xu, H. Yao and J. Hou, *Chin. J. Chem.*, 2019, **37**, 207–215.
23 J. Zhang, H. S. Tan, X. Guo, A. Facchetti and H. Yan, *Nat. Energy*, 2018, **3**, 720–731.

24 P. Cheng, G. Li, X. Zhan and Y. Yang, *Nat. Photonics*, 2018, **12**, 131–142.
25 Y. Chen, X. Wan and G. Long, *Acc. Chem. Res.*, 2013, **46**, 2645–2655.
26 W. Zhao, S. Li, H. Yao, S. Zhang, Y. Zhang, B. Yang and J. Hou, *J. Am. Chem. Soc.*, 2017, **139**, 7148–7151.
27 Z. Fei, F. D. Eisner, X. Jiao, M. Azzouzi, J. A. Rohr, Y. Han, M. Shahid, A. S. R. Chesman, C. D. Easton, C. R. McNeill, T. D. Anthopoulos, J. Nelson and M. Heeney, *Adv. Mater.*, 2018, **30**, 1705209.
28 J. Sun, X. Ma, Z. Zhang, J. Yu, J. Zhou, X. Yin, L. Yang, R. Geng, R. Zhu, F. Zhang and W. Tang, *Adv. Mater.*, 2018, **30**, 1707150.
29 D. He, F. Zhao, J. Xin, J. J. Rech, Z. Wei, W. Ma, W. You, B. Li, L. Jiang, Y. Li and C. Wang, *Adv. Energy Mater.*, 2018, **8**, 1802050.
30 W. Liu, J. Zhang, Z. Zhou, D. Zhang, Y. Zhang, S. Xu and X. Zhu, *Adv. Mater.*, 2018, **30**, 1800403.
31 C. Huang, X. Liao, K. Gao, L. Zuo, F. Lin, X. Shi, C.-Z. Li, H. Liu, X. Li, F. Liu, Y. Chen, H. Chen and A. K. Y. Jen, *Chem. Mater.*, 2018, **30**, 5429–5434.
32 R. J. Ming, J. X. Wang, W. Gao, M. Zhang, J. H. Gao, W. M. Ning, Z. H. Luo, X. H. Liu, C. Zhong, F. J. Zhang and C. L. Yang, *Small Methods*, 2019, **3**, 1900280.
33 Y. Lin, J. Wang, Z. G. Zhang, H. Bai, Y. Li, D. Zhu and X. Zhan, *Adv. Mater.*, 2015, **27**, 1170–1174.
34 W. Zhao, D. Qian, S. Zhang, S. Li, O. Inganas, F. Gao and J. Hou, *Adv. Mater.*, 2016, **28**, 4734–4739.
35 N. Qiu, H. Zhang, X. Wan, C. Li, X. Ke, H. Feng, B. Kan, H. Zhang, Q. Zhang, Y. Lu and Y. Chen, *Adv. Mater.*, 2017, **29**, 1604964.
36 T. Liu, Z. H. Luo, Y. Z. Chen, T. Yang, Y. Q. Xiao, G. Y. Zhang, R. J. Ma, X. H. Lu, C. L. Zhan, M. J. Zhang, C. L. Yang, Y. F. Li, J. N. Yao and H. Yan, *Energy Environ. Sci.*, 2019, **12**, 2529.
37 Y. Dong, Y. Zou, J. Yuan, H. Yang, Y. Wu, C. Cui and Y. Li, *Adv. Mater.*, 2019, **31**, 1904601.
38 T.-W. Chen, K.-L. Peng, Y.-W. Lin, Y.-J. Su, K.-J. Ma, L. Hong, C.-C. Chang, J. Hou and C.-S. Hsu, *J. Mater. Chem. A*, 2020, **8**, 1131–1137.
39 Z. Zhou, W. Liu, G. Zhou, M. Zhang, D. Qian, J. Zhang, S. Chen, S. Xu, C. Yang, F. Gao, H. Zhu, F. Liu and X. Zhu, *Adv. Mater.*, 2019, **32**, 1906324.
40 R. Qin, D. Wang, G. Zhou, Z.-P. Yu, S. Li, Y. Li, Z.-X. Liu, H. Zhu, M. Shi, X. Lu, C.-Z. Li and H. Chen, *J. Mater. Chem. A*, 2019, **7**, 27632–27639.
41 C. Sun, S. Qin, R. Wang, S. Chen, F. Pan, B. Qiu, Z. Shang, L. Meng, C. Zhang, M. Xiao, C. Yang and Y. Li, *J. Am. Chem. Soc.*, 2020, **142**, 1465–1474.
42 G. F. Burkhard, E. T. Hoke and M. D. McGehee, *Adv. Mater.*, 2010, **22**, 3293–3297.
43 W. Shockley and H. J. Queisser, *J. Appl. Phys.*, 1961, **32**, 510–519.
44 B. Kan, H. Feng, H. Yao, M. Chang, X. Wan, C. Li, J. Hou and Y. Chen, *Sci. China: Chem.*, 2018, **61**, 1307–1313.
45 Z. H. Zhang, X. Liu, J. S. Yu, H. T. Wang, M. Zhang, L. A. Yang, R. Y. Geng, J. R. Cao, F. A. Du, F. Liu and W. H. Tang, *J. Mater. Chem. C*, 2019, **7**, 13279–13286.
46 D. Qian, Z. Zheng, H. Yao, W. Tress, T. R. Hopper, S. Chen, S. Li, J. Liu, S. Chen, J. Zhang, X. K. Liu, B. Gao, L. Ouyang, Y. Jin, G. Pozina, I. A. Buyanova, W. M. Chen, O. Inganas, V. Coropceanu, J. L. Bredas, H. Yan, J. Hou, F. Zhang, A. A. Bakulin and F. Gao, *Nat. Mater.*, 2018, **17**, 703–709.
47 T. Wang and J.-L. Brédas, *Matter*, 2020, **2**, 119–135.
48 H. Bronstein, C. B. Nielsen, B. C. Schroeder and I. McCulloch, *Nat. Rev. Chem.*, 2020, **4**, 66–77.
49 S. Dai, F. Zhao, Q. Zhang, T. K. Lau, T. Li, K. Liu, Q. Ling, C. Wang, X. Lu, W. You and X. Zhan, *J. Am. Chem. Soc.*, 2017, **139**, 1336–1343.
50 Z. Xiao, S. Yang, Z. Yang, J. Yang, H. L. Yip, F. Zhang, F. He, T. Wang, J. Wang, Y. Yuan, H. Yang, M. Wang and L. Ding, *Adv. Mater.*, 2019, **31**, 1804790.
51 Z. Xiao, X. Jia, D. Li, S. Wang, X. Geng, F. Liu, J. Chen, S. Yang, T. P. Russell and L. Ding, *Sci. Bull.*, 2017, **62**, 1494–1496.
52 Z. Xiao, X. Jia and L. Ding, *Sci. Bull.*, 2017, **62**, 1562–1564.
53 X. Li, H. Huang, Z. Peng, C. Sun, D. Yang, J. Zhou, A. Liebman-Pelaez, C. Zhu, Z.-G. Zhang, Z. Zhang, Z. Xie, H. Ade and Y. Li, *J. Mater. Chem. A*, 2018, **6**, 15933–15941.
54 Y. Zhou, M. Li, J. Song, Y. Liu, J. Zhang, L. Yang, Z. Zhang, Z. Bo and H. Wang, *Nano Energy*, 2018, **45**, 10–20.
55 H. Wu, H. Fan, S. Xu, L. Ye, Y. Guo, Y. Yi, H. Ade and X. Zhu, *Small*, 2019, **15**, 1804271.
56 C. M. Proctor, M. Kuik and T.-Q. Nguyen, *Prog. Polym. Sci.*, 2013, **38**, 1941–1960.
57 Y. Wang, Y. Zhang, N. Qiu, H. Feng, H. Gao, B. Kan, Y. Ma, C. Li, X. Wan and Y. Chen, *Adv. Energy Mater.*, 2018, **8**, 1702870.
58 D. M. Smilgies, *J. Appl. Crystallogr.*, 2009, **42**, 1030–1034.
59 H. Feng, N. Qiu, X. Wang, Y. Wang, B. Kan, X. Wan, M. Zhang, A. Xia, C. Li, F. Liu, H. Zhang and Y. Chen, *Chem. Mater.*, 2017, **29**, 7908–7917.

